Title

Temperature-Dependent Kinetics of the Reactions of the Criegee Intermediate CH2OO with Hydroxyketones.

Authors

Cornwell, Zachary A
Enders, Jonas J
Harrison, Aaron W
et al.

Publication Date

2024-03-01

DOI

10.1021/acs.jpca.4c00156

Temperature-Dependent Kinetics of the Reactions of the Criegee Intermediate CH_2OO with Hydroxyketones

Zachary A. Cornwell,[1] Jonas J. Enders,[1] Aaron W. Harrison,[2] and Craig Murray*,[1]

1. *Department of Chemistry, University of California, Irvine, Irvine CA 92697, USA*
2. *Department of Chemistry, Austin College, Sherman, TX 75090, USA*

* Email: craig.murray@uci.edu; Telephone: +1-949-824-4218

Abstract

Though there is a growing body of literature on the kinetics of CIs with simple carbonyls, CI reactions with functionalized carbonyls such as hydroxyketones remain unexplored. In this work, the temperature-dependent kinetics of the reactions of CH_2OO with two hydroxyketones, hydroxyacetone (AcOH) and 4-hydroxy-2-butanone (4H2B), have been studied using a laser flash photolysis transient absorption spectroscopy technique and complementary quantum chemistry calculations. Bimolecular rate constants were determined from CH_2OO loss rates observed under pseudo-1st order conditions across the temperature range 275–335 K. Arrhenius plots were linear and yielded T-dependent bimolecular rate constants: $k_{AcOH}(T) = (4.3\pm1.7)\times10^{-15}\exp[(1630\pm120)/T]$ and $k_{4H2B}(T) = (3.5\pm2.6)\times10^{-15}\exp[(1700\pm200)/T]$. Both reactions show negative temperature dependences and overall very similar rate constants. Stationary points on the reaction energy surfaces were characterized using the composite CBS-QB3 method. Transition states were identified for both 1,3-dipolar cycloaddition reactions across the carbonyl and 1,2-insertion/addition at the hydroxyl group. The free energy barriers for the latter reaction pathways are higher by ~4–5 kcal mol^{-1}, and their contributions are presumed to be negligible for both AcOH and 4H2B. The cycloaddition reactions are highly exothermic and form cyclic secondary ozonides (SOZs) that are the typical primary products of Criegee intermediate reactions with carbonyl compounds. The reactivity of the hydroxyketones towards CH_2OO appears to be similar to that of acetaldehyde, which can be rationalized by consideration of the energies of the frontier molecular orbitals involved in the cycloaddition. The CH_2OO + hydroxyketone reactions are likely too slow to be of significance in the atmosphere, except at very low temperatures.

Introduction

Criegee intermediates (CIs) are a zwitterionic species formed in alkene ozonolysis that can impact the oxidizing capacity of the troposphere.[1–4] Alkene ozonolysis proceeds via a 1,3-dipolar cycloaddition reaction to produce a cyclic 1,2,3-trioxolane, or primary ozonide (POZ), that promptly decomposes to form a CI and a carbonyl compound.[1,5] While larger CIs tend to undergo unimolecular decomposition,[6,7] generating OH radicals, the smallest CI, CH_2OO, has a longer lifetime and may undergo bimolecular reaction with trace atmospheric gases after collisional stabilization.[8,9] Reaction with water vapor, primarily in the form of water dimer, is the major reactive sink for CH_2OO,[4] although bimolecular reactions with other trace atmospheric gases, such as SO_2 and organic acids, are occasionally competitive in specific environments and under favorable conditions.[4,10]

CIs react with carbonyl species in a concerted 1,3-dipolar cycloaddition reaction to form a cyclic 1,2,4-trioxolane, or secondary ozonide (SOZ). Recently, work in our laboratory has explored the effect of varying the carbonyl substituents (R_1R_2CO, where R_1, R_2 are alkyl or acyl groups) on the gas-phase reactivity of a series of ketones and diketones with CH_2OO.[11,12] Reactivity trends can be rationalized using concepts from frontier molecular orbital (FMO) theory.[13–16] The cycloaddition mechanism arises primarily from π–π^* interactions between the occupied $n(p_C–p_O)$ orbital of the electron rich species (CH_2OO) and the unoccupied π^* orbital of the electron deficient species (R_1R_2CO). Electron withdrawing groups (EWGs) on the carbonyl lower the energy of the carbonyl π^* orbital, which reduces the energy gap with the CI orbital, stabilizes the transition state (TS), and increases reactivity. Electron donating groups (EDGs) have the opposite effect, and ultimately decrease reactivity. Hammett substituent constants provide a useful qualitative proxy for the electron-donating or withdrawing-character of the substituents on the carbonyl.[17,18]

The kinetics of the reaction of acetone (Ac, $R_1 = R_2 = CH_3$), a representative model ketone, with CH_2OO has been thoroughly investigated experimentally,[11,12,19–22] with recent measurements converging on

a 298 K rate constant of ~5×10^{-13} cm^3 s^{-1}. Aldehydes (R_1 = H, R_2 = H or alkyl) react faster, with rate constants in the range $(1–4)\times10^{-12}$ cm^3 s^{-1}.[19,20,23–25] The presence of strongly electron withdrawing groups increases rate constants further. For example, hexafluoroacetone (HFA, $R_1 = R_2 = CF_3$) has a rate constant of ~3×10^{-11} cm^3 s^{-1}.[19,26] The α-diketones, biacetyl (BiAc, $R_1=CH_3$, $R_2 = CH_3CO$) and acetyl propionyl (AcPr, $R_1 = CH_3/C_2H_5$), have both electron-donating alkyl and electron-withdrawing acyl substituents, and the reactions ~1×10^{-11} cm^3 s^{-1}.[11,12] Where examined, all reactions of carbonyls with CH_2OO show a negative temperature dependence.

Our focus in this study is the reactions of CH_2OO with two hydroxyketones: hydroxyacetone (acetol, AcOH, $R_1 = CH_3$, $R_2 = CH_2OH$) and 4-hydroxy-2-butanone (4H2B, $R_1 = CH_3$, $R_2 = CH_2CH_2OH$). Hydroxyketones are multifunctional VOCs, which present multiple reactive sites and may exhibit cooperative effects.[27] The reactions of AcOH and 4H2B with CH_2OO can occur at the carbonyl or the hydroxyl moieties. The latter pathway is expected to be minor, as aliphatic alcohols react with CH_2OO to form alkoxymethyl hydroperoxides, with rate constants in the range $(1–2)\times10^{-13}$ cm^3 s^{-1} at 298 K,[28,29] smaller than those of most carbonyls. The hydroxymethyl (CH_2OH) group has Hammett substituent constants of zero, and is neither electron-donating nor withdrawing. Consequently, the rate constant for the cycloaddition reaction is anticipated to be comparable to that of acetaldehyde.

AcOH and 4H2B have also been identified as trace gases in the troposphere,[30,31] where they are formed as secondary oxidation products of isoprene and other atmospheric hydrocarbons.[32–35] AcOH is also produced directly from biomass burning.[36,37] The major reactive sink for hydroxyketones is reaction with OH radicals, which results in lifetimes of a few days. Kinetics studies of the OH + AcOH reaction have produced surprisingly inconsistent results; the IUPAC recommendation for the 298 K rate constant is 5.9×10^{-12} cm^3 s^{-1}.[38–47] The OH + 4H2B kinetics measurements show similar inconsistencies, but the 298 K rate constant appears to be similar.[40,48–52] Photolysis of both species is far slower than reaction with OH, particularly for AcOH where the presence of the α-hydroxyl group

causes a ~10 nm blue shift of the first absorption band that reduces the absorption at actinic wavelengths (see Figure S2 in the Supporting Information).[53]

The results of laser flash photolysis transient absorption spectroscopy measurements quantifying the temperature-dependent kinetics of the reactions of CH_2OO with AcOH and 4H2B across the range 275–335 K are reported here. Complementary *ab initio* calculations map out the reaction energy profiles and provide a basis for explaining reactivity trends using frontier molecular orbital theory. The potential implications of the title reactions in the atmosphere are briefly discussed.

Methods

The temperature-controlled flash photolysis, transient absorption spectroscopy apparatus has been described in detail previously,[12] and will be summarized briefly here.

CH_2OO was produced in the flow reactor by the photolysis of diiodomethane (CH_2I_2) in the presence of excess O_2 using the 355 nm output of an Nd:YAG laser (Continuum Surelite II-10). Typical pulse energies were ~10 mJ, resulting in fluences of ~28 mJ cm^{-2}. Absorption spectra were obtained by dispersing the output of pulsed LEDs (LightSpeed Technologies) in a spectrograph (Andor Shamrock 303i with iDus 420 CCD camera). Kinetics measurements used an LED nominally centered at 365 nm to obtain transient absorption spectra of CH_2OO (and IO) in the range 360–395 nm at various time delays after photolysis. Independent absorption measurements were performed in the range 270–295 nm using an LED centered at 280 nm to quantify reactant concentrations. A digital delay generator (Quantum Composers, 9528) synchronized the photolysis laser, LED driver, and CCD camera.

The flow reactor itself comprises a jacketed quartz tube, with an effective path length of 90 cm. A unistat (Huber Tango) precisely controlled the reactor temperature (within < 1 K) over the range 275–335 K. Gas flows into the reactor were controlled using a range of choked-flow orifices (O'Keefe).

Gases (O_2 and N_2) were used directly from the cylinders, while liquids (CH_2I_2, AcOH, and 4H2B) were placed in smog bubblers and carried into the cell by a flow of N_2. The smog bubblers were held in a water bath maintained at 295 K to prevent evaporative cooling and vapor pressure drop off. Measurements with AcOH used a total flow rate of 3.8 sLpm, resulting in a pressure of 78 Torr in the reactor. The lower vapor pressure of 4H2B (1.2 Torr versus 3.5 Torr at 295 K)[49,54] required a larger total flow rate of 4.9 sLpm and a reactor pressure of 100 Torr. Typically, the concentrations in the reactor were $[CH_2I_2] = 1.1\times10^{15}$ cm^{-3}, $[O_2] = 2.1\times10^{17}$ cm^{-3}, [AcOH] = (1–5)×10^{15} cm^{-3}, [4H2B] = (0.5–1.5)×10^{15} cm^{-3}, with N_2 balance. All chemicals were used as supplied: O_2 (Airgas, UHP 4.4), N_2 (Airgas, industrial grade), CH_2I_2 (Sigma Aldrich, 99%), AcOH (Acros Organics, 90%), and 4H2B (Tokyo Chemical Industry, 95%). FT-IR spectra of the headspace above samples of liquid AcOH and 4H2B were recorded (see Figure S1 in Supporting Information) using a JASCO 4700 spectrometer to identify any impurities. No bands associated with any other organic species were identified, consistent with previous suggestions that the likely impurity in AcOH is residual H_2O,[55] although at levels too low to affect the kinetics measurements.

Electronic structure calculations were performed with the GAMESS and Gaussian 16 programs.[56–59] Geometries of reactants, products, entrance channel complexes, and transition state structures were initially optimized using the B3LYP functional with the Dunning-type cc-pVDZ basis set and the harmonic frequencies subsequently calculated. The presence of zero or one imaginary frequency confirmed that the optimized geometries were true minima or transition states (TSs), respectively. Intrinsic reaction coordinate (IRC) calculations were performed to verify that the expected reactants and products were reached on either side of the TS. Reaction thermochemistry was determined using rigid-rotor harmonic-oscillator (RRHO) partition functions. Additional calculations were performed using the composite CBS-QB3 method to refine the calculated energies.[60] The CBS-QB3 method provides reliable thermochemistry at modest computational cost.[61–63] In addition, the frontier molecular orbital energies are obtained from the optimization output at the B3LYP/cc-pVDZ level of

theory. Previous work has shown the frontier orbital energies calculated at a similar level of theory to provide linear correlation with molecular properties such ionization potential, electron affinity, and excitation energy.[64]

Results

Reactant Concentration Measurements

As in our previous work,[11,12,28] concentrations of the hydroxyketone reactants in the flow cell during kinetics measurements can be estimated using reported vapor pressures (3.50±0.17 Torr for AcOH, and 1.24±0.04 Torr for 4H2B)[49,54] and fractional flow rates. Since the first UV absorption bands of both hydroxyketones can be observed using an LED centered at 280 nm,[53] their concentrations can also be measured directly. Absorption spectra of the hydroxyketones are recorded in the wavelength range 275–290 nm under conditions that are otherwise identical to those used in the kinetics measurements across the 275–335 K temperature range. Absolute hydroxyketone number densities are determined using previously reported absorption cross sections. The first UV absorption bands of AcOH and 4H2B have peak cross sections of ~6×10^{-20} cm^2 at ~270 nm and 280 nm respectively, as is typical of the excitation to the $S_1(n\pi^*)$ state in carbonyls.[53] The only reported measurement for 4H2B is by Messaadia et al,[65] while various measurements exist for AcOH.[39,42,53,65] There is a discrepancy between the AcOH cross sections recommended by the IUPAC Task Group on Atmospheric Chemical Kinetic Data Evaluation and JPL Chemical Kinetics and Photochemical Data for Use in Atmospheric Studies Evaluation.[47,66] While IUPAC prefers the values of Orlando et al,[39] JPL uses an average of that and lower values measured by Butkovskaya et al.[39,42] Since the other reported measurements agree well with the JPL recommendation,[53,65] we elect to use it to quantify $[AcOH]_{exp}$ and determine a concentration scale factor. The UV absorption spectra of both hydroxyketones are shown in Figure S2 in the Supporting Information.

The gradients of plots of measured against estimated concentrations ($[X]_{exp}$ vs. $[X]_{est}$) (Figure S3 and S4 in the Supporting Information) provide a scaling factor that can be used to correct the estimated hydroxyketone concentrations. Previously,[11,12] we have found concentration scaling factor values within 10% of unity for acetone and diketones, indicating that the estimates give values close to the actual concentrations in the flow cell. The hydroxyketone concentration scaling factors deviate from unity, however, as can be seen from Figure 1. For AcOH, the scale factor is independent of temperature with an average value of 1.23±0.07, indicating that the actual concentration is slightly higher than estimated. In contrast, the values determined for 4H2B suggest that its concentration is overestimated, with an average 0.59±0.08. The overall uncertainties are estimated from the spread in values obtained in multiple measurements across the temperature range.

Deviations from unity for the concentration scaling factors derive primarily from systematic errors in $[X]_{est}$ and/or $[X]_{exp}$, which depend respectively on the hydroxyketone vapor pressures $P_{vap,X}$ and absorption cross sections $\sigma_X(\lambda)$. The T-dependent vapor pressures of AcOH and 4H2B have been measured to a high degree of precision,[49,54] although several groups have discussed evidence of hydroxyketone "stickiness" in the course of kinetics measurements.[43,44,65] Wall losses between the bubbler and the flow reactor would lead to concentration overestimates and scaling factors <1, which is consistent with the observed value for 4H2B but not for AcOH. Based on the FT-IR spectrum of AcOH shown in Figure S1 in the Supporting Information and reported band intensities,[36] we estimate a vapor pressure of 3.9±0.4 Torr. If the C=O stretch bands of AcOH and 4H2B are assumed to have the same intensity (as supported by *ab initio* calculations) we estimate the vapor pressure of 4H2B to be 0.76±0.11 Torr. The ratios of these estimated vapor pressures to the literature values[49,54] are 1.11±0.12 for AcOH and 0.61±0.09, in good agreement with the measured scaling factors and suggesting that the systematic error originates in the reported values of $P_{vap,X}$. Another possibility for values <1 is that the smog bubbler headspace is not saturated with the organic vapor, although the use of the experimental scale factor corrects for this effect.

For the purposes of the kinetics measurements, the absorption cross sections are ultimately of most significance as they are used to determine $[X]_{exp}$ directly. As noted above, $\sigma_{AcOH}(\lambda)$ values recommended by IUPAC are 10% greater than the JPL values, which would produce lower values of $[AcOH]_{exp}$ and bring the concentration scaling factor value closer to unity (1.12±0.06) and closer to the vapor pressure ratio estimated from the FT-IR spectra. Such a change would also require an increase in the bimolecular rate constant for reaction with CH_2OO proportionally. We proceed on the basis that the $\sigma_X(\lambda)$ values used are accurate. The rate constants determined in the experiments discussed below are inversely proportional to $\sigma_X(\lambda)$ and can be adjusted appropriately if improved values become available in the future.

Kinetics Measurements

The kinetics of the reactions of CH_2OO with AcOH and 4H2B were studied under pseudo-1st order conditions of excess hydroxyketone at four temperatures in the range 275–335 K. The lowest hydroxyketone concentrations were approximately two orders of magnitude greater than $[CH_2OO]_0$. Transient absorption spectra obtained in the range 363–395 nm at various photolysis-probe delay times were decomposed into contributions from CH_2OO and IO using known absorption spectra[67,68] to generate $[CH_2OO]_t$ and $[IO]_t$ concentration-time profiles. Examples of typical experimental transient spectra recorded with and without AcOH and the resulting $[CH_2OO]_t$ profiles are shown in Figure S5 in the Supporting Information. As expected, the CH_2OO concentrations are observed to decrease more rapidly with increasing hydroxyketone concentration, while the IO concentration profiles remain unaffected. Peak Criegee intermediate concentrations of $[CH_2OO]_0 = (6–8)\times10^{12}$ cm^{-3} are significantly smaller than those of the hydroxyketone reactants, ensuring pseudo-1st order conditions.

Analysis of the $[CH_2OO]_t$ profiles used the same kinetic model as described previously and summarized in Supporting Information.[11,12] The differential rate law for CH_2OO loss includes a

quadratic term for bimolecular self-reaction with rate constant k_{self} and a linear term for pseudo-1st order reactions with rate constant k_{loss}. The pseudo-1st order rate constants k_{loss} at each hydroxyketone concentration are derived from fits of the $[CH_2OO]_t$ profiles to the integrated rate law, with k_{self} fixed to a T-independent value of 7.8×10^{-11} cm^3 s^{-1}.[12] Plots of k_{loss} against [hydroxyketone] are linear and a least-squares fit (weighted by the uncertainties in both k_{loss} and [hydroxyketone]) returns a background loss rate k_{bgd} and the bimolecular rate constant $k_{hydroxyketone}$ as the gradient. Examples are shown in Figure 2 for the reactions of CH_2OO with AcOH and 4H2B at 295 K and the full set of measurements at all four temperatures is shown in Figures S6 and S7 in the Supporting Information. At 295 K, the bimolecular rate constants for the CH_2OO + AcOH and CH_2OO + 4H2B reactions are the same within the statistical uncertainties of the fits: $k_{AcOH} = (1.09\pm0.15)\times10^{-12}$ cm^3 s^{-1} and $k_{4H2B} = (1.11\pm0.26)\times10^{-12}$ cm^3 s^{-1}. As has been observed for other reactions of CH_2OO with carbonyl species,[12,20,22,25] the rate constants for the AcOH and 4H2B reactions also decrease with increasing temperature. The complete set of measured T-dependent rate constants are summarized in Table 1. Background loss rates, attributed to reaction with I atoms or other species present in the flow reactor, are typically between ~1000–1500 s^{-1} and decrease slightly with increasing temperature. The bimolecular rate constants for the CH_2OO + hydroxyketone reactions were obtained by averaging three individual kinetic runs at each temperature, with errors representing the statistical uncertainty (1σ) in the fit. The same values, although with smaller uncertainties, are obtained from global fits to the complete data sets at each temperature.

Arrhenius plots for both reactions are shown in Figure 3. The plots are linear over the temperature range explored in the experiments and the T-dependent bimolecular rate constants can be expressed in Arrhenius form as $k_{AcOH}(T) = (4.3\pm1.7)\times10^{-15}\exp[(1630\pm120)/T]$ and $k_{4H2B}(T) = (3.5\pm2.6)\times10^{-15}\exp[(1700\pm200)/T]$. The similarity of the $-E_a/R$ values indicates both reactions are equally sensitive to temperature, within the 1σ experimental uncertainties, with negative energies of activation of $E_a \approx -3.3$ kcal mol^{-1}.

The thermodynamic formulation of canonical transition state theory (CTST) for a bimolecular gas-phase reaction can be used to extract the standard entropy, enthalpy, free energy of activation:

$$k = \frac{k_B^2}{hp^\circ} \exp\left(\frac{\Delta^\ddagger S^\circ}{R}\right) T^2 \exp\left(-\frac{\Delta^\ddagger H^\circ}{RT}\right)$$

The factor k_B^2/hp° is evaluated to be 2.87×10^{-12} cm^3 s^{-1} K^{-2} using $p^\circ = 10^5$ Pa. $\Delta^\ddagger S^\circ$ and $\Delta^\ddagger H^\circ$ are the standard entropy and enthalpy of activation, respectively. The latter is related to the activation energy by $\Delta^\ddagger H^\circ = E_a - 2RT$ for a bimolecular reaction.[69] Unsurprisingly, given the similarities in the T-dependent rate constants, the thermodynamic parameters derived for the AcOH and 4H2B reactions are also similar, with $\Delta^\ddagger S^\circ \approx -40$ cal K^{-1} mol^{-1}, $\Delta^\ddagger H^\circ \approx -4.5$ kcal mol^{-1}, and $\Delta^\ddagger G^\circ \approx +7.3$ kcal mol^{-1} at 298 K. The pre-exponential factors, activation energies, and thermodynamics of activation for AcOH and 4H2B are compiled in Table 1. An alternative analysis using linear least-squares fits of ln (k/T^2) vs. $1/T$, shown in Figure S8 and Table S1 in Supporting Information, yields identical thermodynamic parameters within the experimental uncertainties.

The pressure dependence of the CH_2OO + hydroxyketone reactions was also investigated by measuring k_{loss} across the range 80–120 Torr range at 295 K and using a single concentration of each hydroxyketone ([AcOH] = $(5.1\pm0.3)\times10^{15}$ cm^{-3} and [4H2B] = $(8.0\pm1.1)\times10^{14}$ cm^{-3}). The total pressure was changed by varying the flow rate of the N_2 buffer gas, while leaving all other flow rates unchanged. The average k_{loss} values as a function of total pressure are shown in Figure S9 in Supporting Information. No change in k_{loss} is observed as the total pressure is varied and the average values are the same as those obtained in the kinetics measurements. Based on similar measurements for the CH_2OO + Ac reaction,[12,22] we conclude that the rate constants measured in 80–100 Torr of N_2 likely represent the high-pressure limit.

Computational Results

We have performed ab initio calculations to characterize the reactions of CH_2OO with AcOH and 4H2B. Geometries of the reactants, entrance channel complexes, transition states (TSs), and primary products were optimized, initially at the B3LYP/cc-pVDZ level of theory, and harmonic frequency analysis performed to confirm minima and saddle points. Intrinsic reaction coordinate calculations were performed to ensure that the TSs connected the reactant and product minima. Subsequent calculations were performed at the CBS-QB3 level of theory to provide improved thermochemistry. The Cartesian coordinates and energies for all species are compiled in the Supporting Information and the CBS-QB3 thermochemistry data, $\Delta(E+\mathrm{ZPE})$ at 0 K and $\Delta H°$, $\Delta G°$ at 298 K, is summarized in Table 2.

Preliminary calculations at the B3LYP/cc-pVDZ level of theory were performed to assess the possible relevance of different hydroxyketone conformers. Four low-energy conformers were identified for each molecule, distinguished primarily by rotations about the α C–C bond and the C–O bond. The optimized geometries are shown in Figure 4. The most stable hydroxyketone conformers are distinguished by the presence of an intramolecular hydrogen bond, resulting in a cyclic five and six membered structures for AcOH and 4H2B, respectively. For both hydroxyketones, the Boltzmann population distribution is dominated at all temperatures (>98%) by the intramolecular H-bonded conformers, which are at least 3 kcal mol^{-1} lower in energy than the next lowest conformer. Higher energy conformers were assumed to play no significant role in the reactions with CH_2OO and were neglected in subsequent calculations.

Hydroxyketones can react with CH_2OO as either carbonyls or alcohols. Reaction at the carbonyl site occurs via a 1,3-dipolar cycloaddition, leading to the formation of a five membered cyclic trioxolane, or secondary ozonide (SOZ). Reaction at the hydroxyl group can occur via a 1,2-addition (or insertion) mechanism, leading to a substituted hydroperoxide. The overall zero-point corrected

energy [Δ(E+ZPE) at 0 K] and Gibbs free energy (ΔG° at 298 K) profiles are shown in Figure 5. The reactions are similarly exoergic with products lying at values of Δ(E+ZPE) ≈ –50 kcal mol^{-1} (ΔG° ≈ –35 kcal mol^{-1}). The entrance channels of both reactions support van der Waals complexes that are bound by 4–9 kcal mol^{-1}, while the TSs have energies that are generally below the separated reactants. On the free energy surface, all entrance channel complexes and TSs are higher in energy than the reactants.

Cycloaddition at the carbonyl site of each hydroxyketone can occur via two near-equivalent pathways that differ in the orientation of the CH_2OO with respect to the OH group of the hydroxyketone. In pathway A, the central O atom of CH_2OO is oriented toward the hydroxyalkyl side at TS_A, while pathway B has the central O oriented towards the methyl side of the hydroxyketone at TS_B. The optimized TS_A and TS_B geometries are shown in Figure 6. Unsurprisingly, the energies and free energies are similar. The free energy barriers for the A and B pathways of the AcOH reaction differ by only 0.2 kcal mol^{-1}, while a difference of 0. 8 kcal is found for the 4H2B reaction, slightly favoring TS_B. The larger energy difference for 4H2B arises because of a geometrical distortion of the hydroxyethyl group out of the plane, away from the attacking CH_2OO, in TS_A while the carbon backbone maintains planarity in TS_B. The TS free energies for reaction at the OH site of the hydroxyketones are significantly higher than those for the cycloaddition reactions (almost 7 kcal mol^{-1} for the AcOH reaction and ∼4 kcal mol^{-1} higher for the 4H2B reaction), as shown in Figure 5 and Table 2.

Discussion

The CH_2OO + AcOH and CH_2OO + 4H2B reactions are found to have almost identical rate constants across the 275–335 K temperature range studied experimentally, as summarized in Table 1. At room temperature (∼295 K), the rate constants for both reactions are 1.1×10^{-12} cm^3 s^{-1}, which is greater than the reactions of simple ketones by around a factor of two. The rate constant for the CH_2OO +

acetone (Ac) reaction has been measured by various groups, with values in the range k_{Ac} = (2.3–4.8)×10^{-13} cm^3 s^{-1} reported,[11,12,19–22] where the range is likely a consequence of the reaction pressure dependence. Measurements at the high-*P* limit have a weighted average value k_{Ac} = 4.3×10^{-13} cm^3 s^{-1}.[11,12,21,22] The rate constant for the CH_2OO + methylethylketone (MEK) reaction is slightly larger than that of Ac with a value k_{MEK} = 6.4×10^{-13} cm^3 s^{-1}.[70] The room temperature rate constants for the hydroxyketone reactions are much closer to that of acetaldehyde (MeCHO), for which rate constants in the range k_{MeCHO} = (1.0–1.7)×10^{-12} cm^3 s^{-1} have been reported.[23,19,20] The CH_2OO + R_1R_2CO reactions also all show similar negative temperature dependences.

The reactivity of the hydroxyketones towards CH_2OO is increased relative to aliphatic ketones, although the effect is largely insensitive to whether the OH is at the α or β position. The OH group provides an additional site for reaction via the 1,2-addition mechanism that has been characterized for alcohols.[28,29,71,72] In general, alcohols tend to react with CH_2OO much more slowly than carbonyls. For example, the rate constant for the CH_2OO + methanol (MeOH) reaction at room temperature is k_{MeOH} = 1.2×10^{-13} cm^3 s^{-1}.[28,29] The increased rate constant for the hydroxyketones relative to acetone is likely due to enhancement of the 1,3-dipolar cycloaddition mechanism rather than being due to the presence of an additional reaction pathway. We note that synergistic rate constant increases arising from the presence of different functional groups have been demonstrated in other Criegee intermediate reactions. For example, 3-aminopropanol reacts with acetaldehyde oxide, CH_3CHOO, in a concerted double hydrogen atom transfer (DHAT) step, where both the amine and hydroxyl functional groups interact with the CI simultaneously, significantly faster than simple amines or alcohols.[27,73] Additionally, acetylacetone (AcAc), which exists predominantly as its enolone tautomer, has C=O, OH, and C=C sites for reaction with CH_2OO. The CH_2OO + AcAc reaction is twice as fast as CH_2OO + Ac at room temperature (k_{AcAc} = 8.0×10^{-13} cm^3 s^{-1}) and shows a weak temperature dependence ($-E_a/R$ = 460 K) which can be explained in part by the existence of competitive pathways for reaction at both the C=O and C=C sites, where *ab initio* calculations find similar $\Delta^{\ddagger}G°$ values at 298

K.[11,12] Rate constants for CH_2OO + alkene reactions are generally much smaller than for carbonyls,[74] and show a positive temperature dependence. For the AcAc reaction, it appears that the adjacent carbonyl group may enhance the reactivity at the C=C site.

The experimental kinetics observations are supported by the *ab initio* calculations, which show the presence of relatively stable entrance channel complexes followed by TS barriers that are in most cases submerged relative to the reactants, consistent with the negative temperature dependences. Additionally, no dependence on total pressure was observed in the range 80–120 Torr of N_2. A two-step mechanism for either the cycloaddition or 1,2-addition reactions can be written as

$$CH_2OO + R_1R_2C{=}O \rightleftharpoons \text{complex} \quad \text{(R1)}$$

$$\text{complex} \rightarrow \text{products} \quad \text{(R2)}$$

where the products are either SOZs or hydroperoxide species (see Supporting Information). In the high-P limit, equilibrium is established for reaction R1 and the overall rate constant can be represented as $k = k_2K_1$, where $K_1 = k_1/k_{-1}$. From the perspective of transition-state theory, the magnitude of the overall experimental rate constant is largely determined by the standard free energy of activation $\Delta^{\ddagger}G°$ at the TS. The results of the CBS-QB3 ab initio calculations are summarized in Table 2 and Figure 5. Free energy barriers for the cycloaddition reactions at the carbonyl are calculated to be broadly similar (~+6 kcal mol^{-1}) and analysis of the temperature dependence of the rate constants results in values that are in good agreement (see Table 1). In contrast, the calculated free energy barriers for reaction at the hydroxyl group are significantly higher (>10 kcal mol^{-1}). For comparison, the free energy of activation for CH_2OO reacting with methanol is calculated to be $\Delta G°$ = +9.1 kcal mol^{-1} at the same CBS-QB3 level of theory (see Table 2). That is, the energy barrier for reaction at the OH position is even higher in the hydroxyketones than in a simple alcohol like methanol, for which the observed rate constant is an order of magnitude lower. The higher energy

barrier is consistent with the disruption of the intramolecular H-bond in the minimum energy structure of hydroxyketones required for reaction at the hydroxyl group. It is only the slightly higher-energy conformers shown in Figure 4 that can take part in the 1,2-addition with CH_2OO. Consequently, we conclude that the dominant reaction between CH_2OO and the hydroxyketones is the 1,3-dipolar cycloaddition at the C=O reaction site. The presence of the hydroxyl group on either the α or β carbon appears to have no significant effect on the observed rate constants, consistent with the similarity of the calculated free energy barriers.

Previously,[11] we have attempted to rationalize the reactivity trends in 1,3-dipolar cycloaddition reactions between CH_2OO and carbonyl compounds (R_1R_2CO, where R1, R2 are alkyl or acyl substituents) using a frontier molecular orbital (FMO) theory approach.[13–16] Starting with the model of symmetry-allowed orbital interactions developed by Sustmann,[13] the cycloaddition between carbonyl compounds and CH_2OO primarily involves interactions between the out-of-plane π and π* orbitals of CH_2OO and R_1R_2CO. The dominant interaction is between the occupied non-bonding n(p_C–p_O) molecular orbital of the electron rich species CH_2OO (the 1,3-dipole) and the lowest unoccupied π* molecular orbital of the electron deficient carbonyl, R_1R_2CO (the dipolarophile), with energy gap $|\Delta E_A|$. The energy gap $|\Delta E_S|$ between the occupied carbonyl π orbital and the unoccupied π* orbital of CH_2OO is, in general, larger and makes a smaller contribution to the reactivity. The energies of the carbonyl FMOs are affected by the electron-donating or electron-withdrawing nature of the substituents R_1 and R_2. Electron-donating groups (EDGs) on the carbonyl raise the energy of the orbitals, increasing the magnitude of $|\Delta E_A|$, leading to a decreased reactivity. In contrast, electron-withdrawing groups (EWGs) lower the orbital energies and have the opposite effect on reactivity. The orbital interactions are illustrated in Figure 7, which shows the FMOs of CH_2OO, and the carbonyls formaldehyde (HCHO), AcOH, 4H2B, and acetone (Ac), calculated at the B3LYP/cc-pVDZ level of theory.

The EWG or EDG character of the R_1, R_2 substituents can be represented by Hammett substituent constants, σ_m and σ_p, where the subscripts refer to substitution at the meta/para position of benzoic acid.[18] Positive values indicate EWG character and increased reactivity, while negative values indicate EDG character, and reduced reactivity. Among the carbonyls HCHO, AcOH, 4H2B, and Ac, the substituents and their Hammett constants are: H ($\sigma_m = \sigma_p = 0$); CH_3 ($\sigma_m = -0.07$, $\sigma_p = -0.17$), CH_2OH ($\sigma_m = \sigma_p = 0$), while values for CH_2CH_2OH are unknown. Methyl is electron-donating, raising the energies of the frontier orbitals while the others are neither. The effect of the electron-donating methyl groups on the calculated FMO energies is evident in Figure 7 and Table 3. Relative to H, each methyl group substituent increases the carbonyl FMO energies by ~0.4 eV. Based on the calculated orbital energies in Table 3 it is likely that CH_2CHOH is marginally more electron-donating than CH_2OH, due to the presence of the additional methylene group between the hydroxyl and the carbonyl. Although the experimental rate constants were found to be indistinguishable, accounting for the possible systematic error in the UV absorption cross section of AcOH described above would lead to a 10% increase in k_{AcOH}, in line with the expectations of the orbital analysis.

Previously, we showed that the relationship between observed rate constants and calculated orbital energy gaps could be used quantitatively.[11] Figure 8 shows an updated plot of ln k against the magnitude of the orbital energy gap $|\Delta E_A|$, for a range of CH_2OO + R_1R_2CO reactions. Experimental rate constants at room temperature have been obtained from various sources,[11,12,19,22,25,26,70,75,76] and are compiled in Table S2 of Supporting information. The data set includes reactions of CH_2OO with ketones, α-diketones, aldehydes, and α,β-unsaturated enones and enals. Where more than one experimental value is available, the weighted average rate constant is used. Orbital energies have been calculated at the B3LYP/cc-pVDZ level, rather than M06-2X/aug-cc-pVTZ as previously.[11] The effect of the electron-donating or electron-withdrawing character of the R_1, R_2 substituents on the orbital energy gaps and rate constants leads to a strong negative linear correlation. The fastest reaction is with hexafluoroacetone (HFA), which has strongly electron-withdrawing substituents (R_1

= R_2 = CF_3, σ_m = 0.43, σ_p = 0.54) while the slowest reaction is with acetone, which has electron-donating substituents (R_1 = R_2 = CH_3). For species with $R_1 \neq R_2$, such as acetaldehyde (R_1 = H, R_2 = CH_3) or the hydroxyketones, the effect is additive. The α,β-unsaturated carbonyls such as MVK, MACR, ACR, and the enolone form of AcAc are shown in Figure 8 but clearly deviate from the trend and are not included in the fit. The $|\Delta E_A|$ values for these species imply that the reactions with CH_2OO should be much faster than observed experimentally,[11,12,75,76] suggesting that delocalization of the π system reduces the reactivity of the carbonyl. Further work is required to explain the reactivity of α,β-unsaturated carbonyls towards CH_2OO, which deviate from the trend.

Atmospheric Implications

The major reactive sink for hydroxyketones in the atmosphere is reaction with OH radicals. Rate constants for reaction with OH are $2.0\times10^{-12}\exp(-320/T)$ cm^3 s^{-1} and $1.3\times10^{-12}\exp(-400/T)$ cm^3 s^{-1} for AcOH and 4H2B respectively.[47,51] Typical lifetimes for both hydroxyketones reacting with OH radical are ~3 days in the troposphere.[38,39,43,44,49,51] Comparatively, photolysis has a minor contribution with lifetimes of ~12-14 days for AcOH and 26 days for 4H2B.[43,51] Temperature-dependent lifetimes for AcOH and 4H2B were estimated using typical average tropospheric concentrations for CH_2OO and OH. The average CH_2OO concentration was assumed to be 2×10^4 cm^{-3}, although concentrations as high as 1×10^5 cm^{-3} have been reported.[3,77] The average concentration of OH was estimated to be 5×10^6 cm^{-3} during the day and 2×10^5 cm^{-3} at night.[78,79] At 295 K, the hydroxyketone reactions with CH_2OO are insignificant, with estimated lifetimes >500 days. However, the CH_2OO reactions show a strong negative T dependence and may become relatively more important at lower temperatures. While the hydroxyketone loss rates due to CH_2OO increase at lower temperature, with lifetimes of ~80 days at 220 K, OH remains the most important reactive sink for both hydroxyketones across the temperature range, even at night when OH concentrations are markedly lower.

Conclusions

The kinetics of the CH_2OO + AcOH and CH_2OO + 4H2B reactions were measured across the temperature range 275–335 K using a flash photolysis, transient absorption spectroscopy technique. The temperature dependent bimolecular rate constants are k_{AcOH} = (4.3±1.7)×10^{-15}exp[(1630±120)/T] and k_{4H2B} = (3.5±2.6)×10^{-15}exp[(1700±200)/T]. Complementary *ab initio* calculations confirm that both reactions proceed via 1,3-dipolar cycloaddition at the carbonyl to form cyclic secondary ozonides, while reaction at the hydroxyl group via 1,2-addition is insignificant. The increased reactivity of hydroxyketones relative to acetone can be understood from a frontier molecular orbital theory approach, wherein the cycloaddition involves an interaction between the occupied n(p_C–p_O) orbital of the CH_2OO and the unoccupied π* orbital of the carbonyl. Electron-donating or electron-withdrawing substituents increase or decrease the π* orbital energy. Alkyl substituents are electron-donating, which decreases reactivity, while hydroxyalkyl substituents are, like H, neither electron-donating nor electron-withdrawing. A strong inverse correlation is found between the logarithm of the rate constants and the orbital energy gap for a range of R_1R_2CO species. The reactions of CH_2OO with AcOH and 4H2B are unlikely to be significant in the troposphere, where reaction with hydroxyl radicals and photolysis control the hydroxyketone lifetimes.

Supporting Information

Description of calibration procedure; FT-IR spectra of AcOH and 4H2B; UV absorption spectra of AcOH and 4H2B; concentration calibration plots; description of kinetic model; example transient absorption spectra and [CH_2OO] time profile; global pseudo-1st-order plots; plot of ln(k/T^2) against 1/T; experimental values of enthalpy, entropy, and Gibbs free energy of activation; pressure dependence of CH_2OO loss rates; compilation of room temperature rate constants for CH_2OO +

R_1R_2CO reactions; CBS-QB3 cartesian coordinates and energies of the reactants, complexes, transition states, and products.

Acknowledgements

This material is based upon work supported by the National Science Foundation under Grant No. ECS-1905364.

Figures

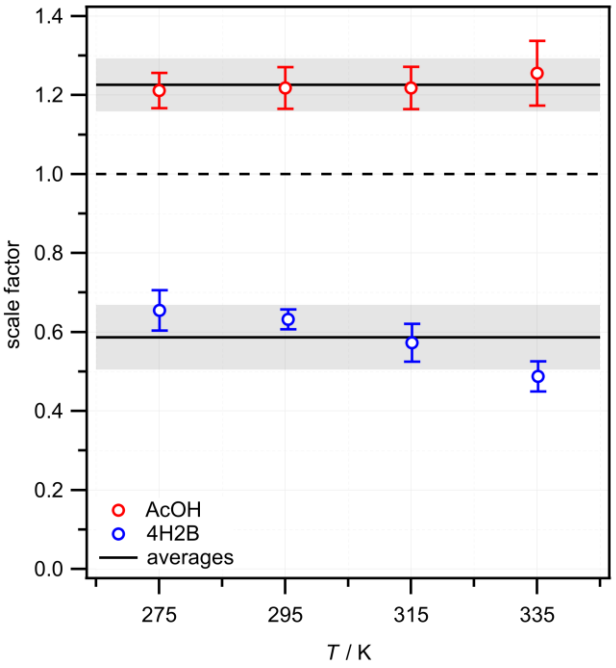

Figure 1 Scale factors determined from gradient of $[X]_{exp}$ versus $[X]_{est}$ calibration plots as a function of temperature. Solid lines are the *T*-independent average, while shaded areas represent the estimated experimental uncertainty, based on the variability of the measurements. Values >1 or <1 indicate that reactant concentration is underestimated (AcOH) or overestimated (4H2B), respectively.

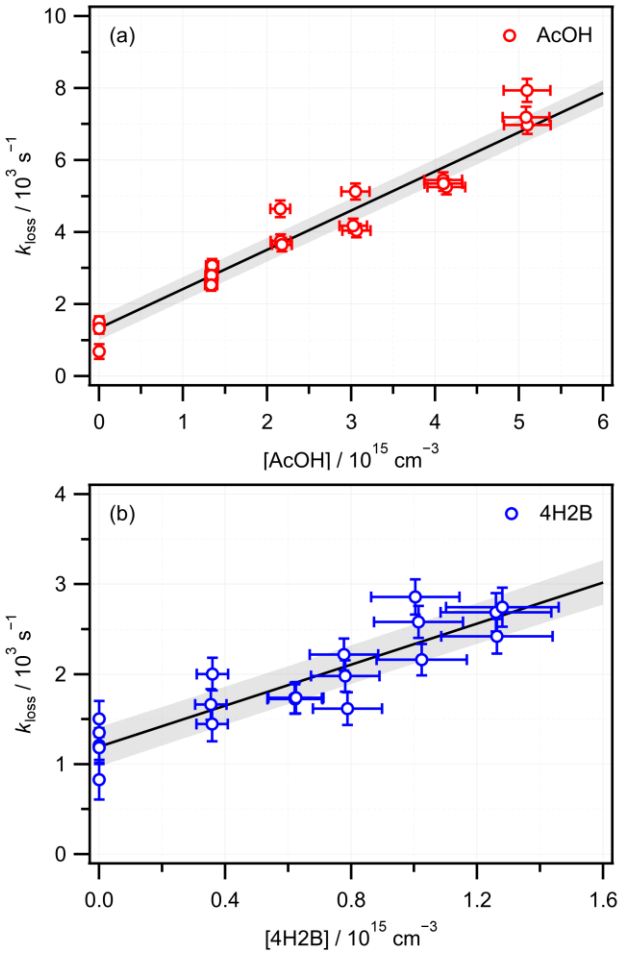

Figure 2 Pseudo-1st order plots for the reactions of CH_2OO with (a) AcOH and (b) 4H2B at 295 K. Vertical and horizontal error bars represent statistical uncertainties (1σ) in the loss rates determined from fitting [CH_2OO] time profiles and uncertainties in the hydroxyketone concentration calibration measurements, respectively. Weighted linear fits to the experimental data are also shown, with shaded area representing 1σ prediction bands.

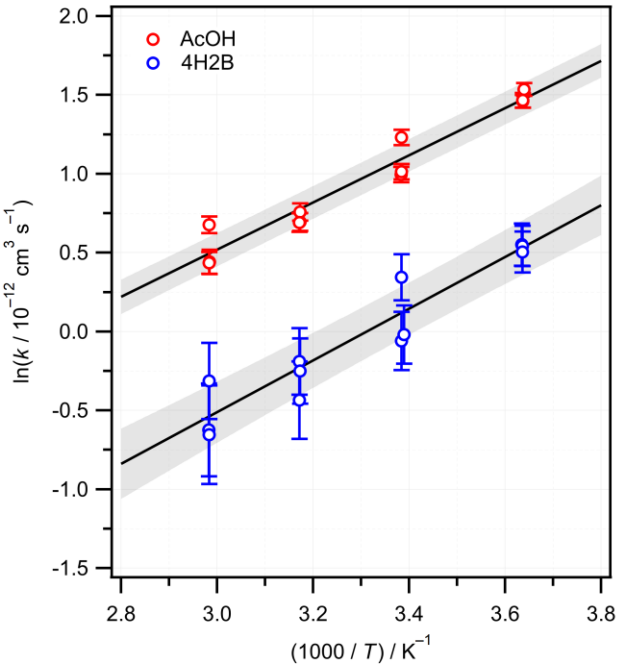

Figure 3 Arrhenius plots for the reaction of CH_2OO with AcOH (red) and 4H2B (blue), with 1σ statistical uncertainties. The AcOH data has been offset vertically for clarity. Solid black lines are linear fits with shaded areas representing 1σ prediction bands.

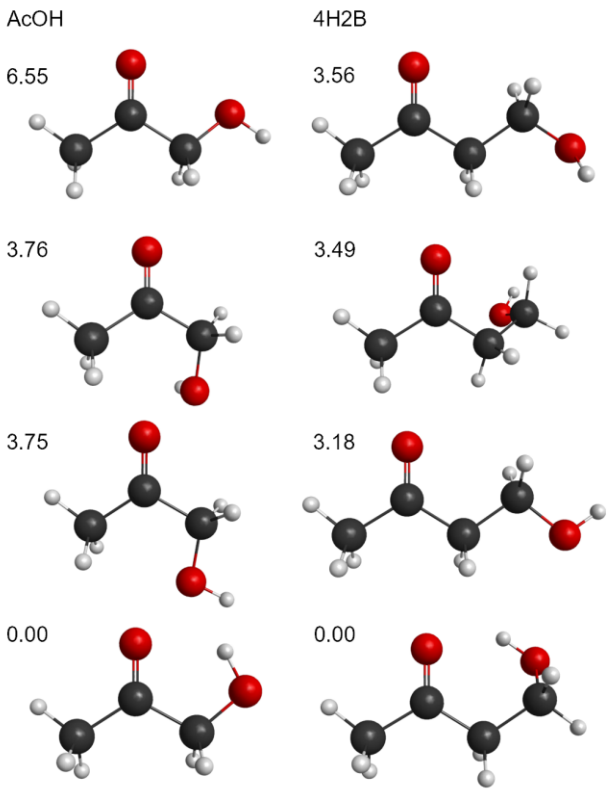

Figure 4 Low-energy conformers of AcOH (left) and 4H2B (right), calculated at the B3LYP/cc-pVDZ level. The zero-point corrected energy (kcal mol^{-1}) of each conformer relative to the most stable cyclic H-bonded structures is indicated.

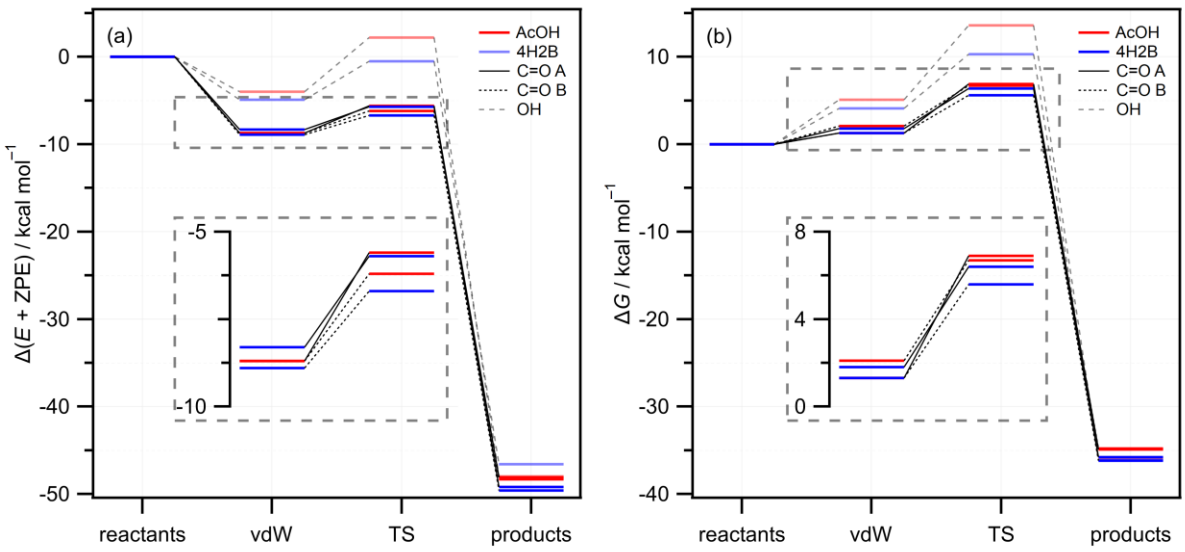

Figure 5 CBS-QB3 energy and free energy profiles for the CH_2OO + AcOH (red) and 4H2B (blue). Panel (a) shows $\Delta(E$+ZPE) at 0 K and panel (b) shows ΔG at 298 K for both reactions. Solid lines connect stationary points for cycloaddition A, dotted lines for cycloaddition B, and dashed lines for 1,2-addition at the OH group. The inset shows a magnified view of the entrance channel van der Waals complex (vdW) and the transition state (TS) for the cycloaddition pathways.

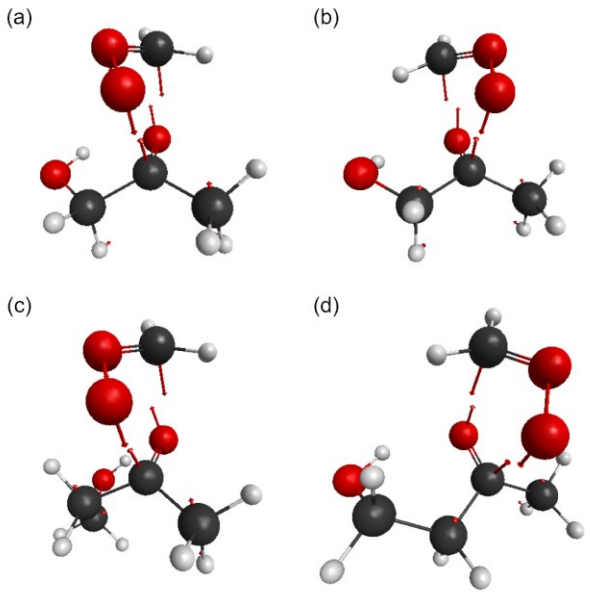

Figure 6 Optimized transition state geometries for the 1,3-dipolar cycloaddition reactions of CH_2OO with AcOH (a, b) and 4H2B (c, d). The orientation of the central O atom of CH_2OO oriented towards (a,c) or away (b,d) from the hydroxyl group of the hydroxyketone identifies cycloaddition A or B, respectively. Red arrows indicate displacement vectors along the reaction coordinate.

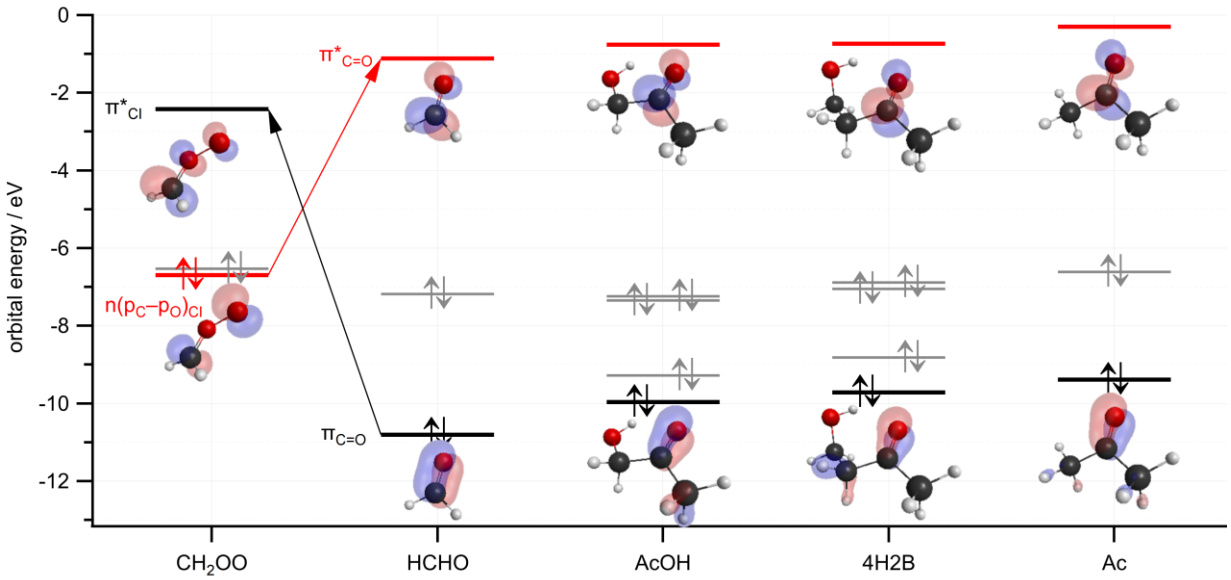

Figure 7 Frontier orbital energies calculated at B3LYP/cc-pVDZ level for CH_2OO and the carbonyls formaldehyde, acetone, and the hydroxyketones AcOH and 4H2B. Red: A orbitals (non-bonding $n(p_C–p_O)$ for CH_2OO, π* LUMO for carbonyls), black: S orbitals (π bonding orbitals of carbonyls, π* antibonding for CH_2OO), gray: non-bonding (n_O orbitals).

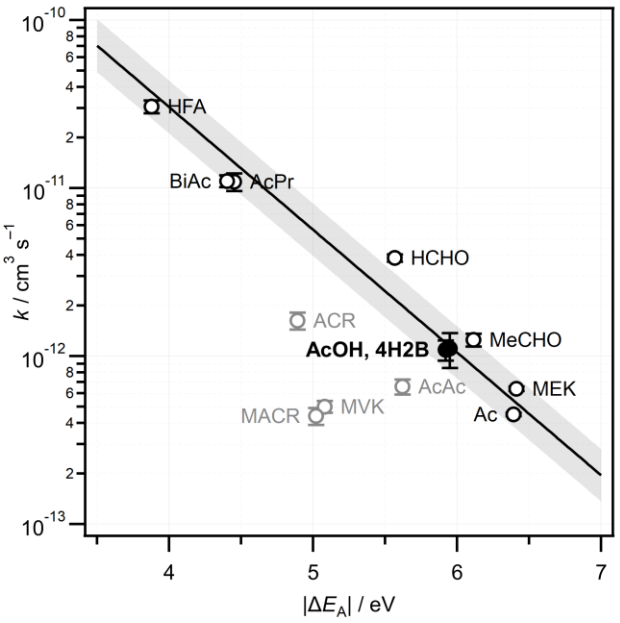

Figure 8 Inverse correlation between reported experimental rate constants at room temperature for the reactions of CH_2OO with a series of carbonyl compounds and the energy gap $|\Delta E_A|$ between the π^* orbital of the carbonyl and the $n(p_C-p_O)$ orbital of CH_2OO. Orbital energies were calculated at the B3LYP/cc-pVDZ level. A linear fit is shown, where the shaded area represents 1σ prediction bands. Experimental rate constants are drawn from various sources – see text for details. Reactions involving α,β-unsaturated carbonyls (gray) were excluded from the fit.

Tables

Table 1 *T*-dependent bimolecular rate constants, Arrhenius parameters, and standard enthalpies, entropies, and Gibbs energies of activation at 298 K for the reactions of CH_2OO with hydroxyacetone and 4H2B. Uncertainties are 1σ statistical uncertainties from the fits.

T / K	k_{AcOH} /10^{-12} cm^3 s^{-1}	k_{4H2B} / 10^{-12} cm^3 s^{-1}
275	1.63±0.07	1.70±0.04
295	1.09±0.15	1.11±0.26
315	0.75±0.03	0.75±0.09
335	0.62±0.09	0.60±0.12
A / 10^{-15} cm^3 s^{-1}	4.3±1.7	3.5±2.6
E_a/R / K	−1630±120	−1700±200
E_a / kcal mol^{-1}	−3.24±0.23	−3.38±0.40
$\Delta^{\ddagger}H°$ / kcal mol^{-1}	−4.43±0.23	−4.56±0.40
$\Delta^{\ddagger}S°$ / cal K^{-1} mol^{-1}	−39.5±0.4	−39.9±0.7
$\Delta^{\ddagger}G°$ / kcal mol^{-1}	+7.36±0.26	+7.34±0.46

Table 2 CBS-QB3 thermochemistry for the reactions of CH_2OO with AcOH and 4H2B: ΔE+ZPE @ 0K ($\Delta H°$ @298 K) [$\Delta G°$@ 298 K] in kcal mol^{-1}.

		cycloaddition A	cycloaddition B	1,2-addition
AcOH	vdW	–8.7 (–8.3) [+1.3]	–8.7 (–8.5) [+2.1]	–4.0 (–3.7) [+5.1]
	TS	–5.6 (–6.5) [+6.9]	–6.2 (–7.2) [+6.7]	+2.2 (+1.4) [+13.6]
	product	–48.1 (–49.5) [–34.9]	–48.3 (–49.8) [–34.8]	–48.0 (–48.9) [–35.9]
4H2B	vdW	–8.3 (–8.0) [+1.8]	–8.9 (–8.6) [+1.3]	–4.9(–4.6) [+4.1]
	TS	–5.7 (–6.5) [+6.4]	–6.7 (–7.6) [+5.6]	–0.5 (–1.1) [+10.3]
	product	–49.2 (–50.6) [–35.8]	–49.6 (–51.0) [–36.2]	–46.6 (–46.9) [–36.1]
Ac	TS	–6.1 (–6.4) [+5.5]		–
MeOH	TS	–	–	–2.0 (–3.1) [+9.1]

Table 3 B3LYP/cc-pVDZ calculated orbital energies (eV) of HCHO, AcOH, 4H2B, and Ac. CH_2OO π* E = –2.422 eV, n(pC–pO) E = –6.694 eV. $|\Delta E_A|$ is the magnitude of the energy difference between the occupied π orbital of CH_2OO and unoccupied π*of the carbonyl (dominant). $|\Delta E_S|$ is the magnitude of the difference between the unoccupied π* orbital of CH_2OO and the occupied π orbital of the carbonyl. The $|\Delta E_A|$ interaction is always smaller.

	HCHO	AcOH	4H2B	Ac
π*	–1.116	–0.762	–0.735	–0.299
$\|\Delta E_A\|$	5.578	5.932	5.959	6.395
π	–10.803	–9.959	–9.714	–9.388
$\|\Delta E_S\|$	6.980	7.538	7.293	6.966

References

(1) Taatjes, C. A.; Shallcross, D. E.; Percival, C. J. Research Frontiers in the Chemistry of Criegee Intermediates and Tropospheric Ozonolysis. *Phys. Chem. Chem. Phys.* **2014**, *16* (5), 1704–1718. https://doi.org/10.1039/C3CP52842A.

(2) Osborn, D. L.; Taatjes, C. A. The Physical Chemistry of Criegee Intermediates in the Gas Phase. *Int. Rev. Phys. Chem.* **2015**, *34* (3), 309–360. https://doi.org/10.1080/0144235X.2015.1055676.

(3) Khan, M. A. H.; Percival, C. J.; Caravan, R. L.; Taatjes, C. A.; Shallcross, D. E. Criegee Intermediates and Their Impacts on the Troposphere. *Environ. Sci.: Processes Impacts* **2018**, *20* (3), 437–453. https://doi.org/10.1039/C7EM00585G.

(4) Cox, R. A.; Ammann, M.; Crowley, J. N.; Herrmann, H.; Jenkin, M. E.; McNeill, V. F.; Mellouki, A.; Troe, J.; Wallington, T. J. Evaluated Kinetic and Photochemical Data for Atmospheric Chemistry: Volume VII – Criegee Intermediates. *Atmos. Chem. Phys.* **2020**, *20* (21), 13497–13519. https://doi.org/10.5194/acp-20-13497-2020.

(5) Criegee, R. Mechanism of Ozonolysis. *Angew. Chem. Int. Ed. Engl.* **1975**, *14* (11), 745–752. https://doi.org/10.1002/anie.197507451.

(6) Vereecken, L.; Novelli, A.; Taraborrelli, D. Unimolecular Decay Strongly Limits the Atmospheric Impact of Criegee Intermediates. *Phys. Chem. Chem. Phys.* **2017**, *19* (47), 31599–31612. https://doi.org/10.1039/C7CP05541B.

(7) Stephenson, T. A.; Lester, M. I. Unimolecular Decay Dynamics of Criegee Intermediates: Energy-Resolved Rates, Thermal Rates, and Their Atmospheric Impact. *International Reviews in Physical Chemistry* **2020**, *39* (1), 1–33. https://doi.org/10.1080/0144235X.2020.1688530.

(8) Stone, D.; Au, K.; Sime, S.; Medeiros, D. J.; Blitz, M.; Seakins, P. W.; Decker, Z.; Sheps, L. Unimolecular Decomposition Kinetics of the Stabilised Criegee Intermediates CH_2OO and CD_2OO. *Phys. Chem. Chem. Phys.* **2018**, *20* (38), 24940–24954. https://doi.org/10.1039/C8CP05332D.

(9) Peltola, J.; Seal, P.; Inkilä, A.; Eskola, A. Time-Resolved, Broadband UV-Absorption Spectrometry Measurements of Criegee Intermediate Kinetics Using a New Photolytic Precursor: Unimolecular Decomposition of CH_2OO and Its Reaction with Formic Acid. *Phys. Chem. Chem. Phys.* **2020**, *22* (21), 11797–11808. https://doi.org/10.1039/D0CP00302F.

(10) Chhantyal-Pun, R.; Khan, M. A. H.; Taatjes, C. A.; Percival, C. J.; Orr-Ewing, A. J.; Shallcross, D. E. Criegee Intermediates: Production, Detection and Reactivity. *Int. Rev. Phys. Chem.* **2020**, *39* (3), 385–424. https://doi.org/10.1080/0144235X.2020.1792104.

(11) Cornwell, Z. A.; Harrison, A. W.; Murray, C. Kinetics of the Reactions of CH_2OO with Acetone, α-Diketones, and β-Diketones. *J. Phys. Chem. A* **2021**, *125* (39), 8557–8571. https://doi.org/10.1021/acs.jpca.1c05280.

(12) Cornwell, Z. A.; Enders, J. J.; Harrison, A. W.; Murray, C. Temperature-Dependent Kinetics of the Reactions of CH_2OO with Acetone, Biacetyl, and Acetylacetone. *Int. J. Chem. Kinet.* **2023**, *55* (3), 154–166. https://doi.org/10.1002/kin.21625.

(13) Sustmann, R. A Simple Model for Substituent Effects in Cycloaddition Reactions. II. The Diels-Alder Reaction. *Tetrahedron Lett.* **1971**, *12* (29), 2721–2724. https://doi.org/10.1016/S0040-4039(01)96962-X.

(14) Houk, K. N.; Sims, Joyner.; Duke, R. E.; Strozier, R. W.; George, J. K. Frontier Molecular Orbitals of 1,3 Dipoles and Dipolarophiles. *J. Am. Chem. Soc.* **1973**, *95* (22), 7287–7301. https://doi.org/10.1021/ja00803a017.

(15) Houk, K. N. Frontier Molecular Orbital Theory of Cycloaddition Reactions. *Acc. Chem. Res.* **1975**, *8* (11), 361–369. https://doi.org/10.1021/ar50095a001.

(16) Fukui, K. Role of Frontier Orbitals in Chemical Reactions. *Science* **1982**, *218* (4574), 747–754. https://doi.org/10.1126/science.218.4574.747.
(17) Hammett, L. P. The Effect of Structure upon the Reactions of Organic Compounds. Benzene Derivatives. *J. Am. Chem. Soc.* **1937**, *59* (1), 96–103. https://doi.org/10.1021/ja01280a022.
(18) Hansch, Corwin.; Leo, A.; Taft, R. W. A Survey of Hammett Substituent Constants and Resonance and Field Parameters. *Chem. Rev.* **1991**, *91* (2), 165–195. https://doi.org/10.1021/cr00002a004.
(19) Taatjes, C. A.; Welz, O.; Eskola, A. J.; Savee, J. D.; Osborn, D. L.; Lee, E. P. F.; Dyke, J. M.; Mok, D. W. K.; Shallcross, D. E.; Percival, C. J. Direct Measurement of Criegee Intermediate (CH_2OO) Reactions with Acetone, Acetaldehyde, and Hexafluoroacetone. *Phys. Chem. Chem. Phys.* **2012**, *14* (30), 10391–10400. https://doi.org/10.1039/C2CP40294G.
(20) Elsamra, R. M. I.; Jalan, A.; Buras, Z. J.; Middaugh, J. E.; Green, W. H. Temperature- and Pressure-Dependent Kinetics of CH_2OO + CH_3COCH_3 and CH_2OO + CH_3CHO: Direct Measurements and Theoretical Analysis. *Int. J. Chem. Kinet.* **2016**, *48* (8), 474–488. https://doi.org/10.1002/kin.21007.
(21) Berndt, T.; Kaethner, R.; Voigtländer, J.; Stratmann, F.; Pfeifle, M.; Reichle, P.; Sipilä, M.; Kulmala, M.; Olzmann, M. Kinetics of the Unimolecular Reaction of CH_2OO and the Bimolecular Reactions with the Water Monomer, Acetaldehyde and Acetone under Atmospheric Conditions. *Phys. Chem. Chem. Phys.* **2015**, *17* (30), 19862–19873. https://doi.org/10.1039/C5CP02224J.
(22) Chhantyal-Pun, R.; Khan, M. A. H.; Martin, R.; Zachhuber, N.; Buras, Z. J.; Percival, C. J.; Shallcross, D. E.; Orr-Ewing, A. J. Direct Kinetic and Atmospheric Modeling Studies of Criegee Intermediate Reactions with Acetone. *ACS Earth Space Chem.* **2019**, *3* (10), 2363–2371. https://doi.org/10.1021/acsearthspacechem.9b00213.
(23) Stone, D.; Blitz, M.; Daubney, L.; Howes, N. U. M.; Seakins, P. Kinetics of CH_2OO Reactions with SO_2, NO_2, NO, H_2O and CH_3CHO as a Function of Pressure. *Phys. Chem. Chem. Phys.* **2014**, *16* (3), 1139–1149. https://doi.org/10.1039/C3CP54391A.
(24) Liu, S.; Chen, Y.; Jiang, H.; Shi, J.; Ding, H.; Yang, X.; Dong, W. Kinetics for the Reaction of Criegee Intermediate CH_2OO with n-Butyraldehyde and Its Atmospheric Implications. *Atmos. Environ.* **2023**, *311*, 120012. https://doi.org/10.1016/j.atmosenv.2023.120012.
(25) Luo, P.-L.; Chen, I.-Y.; Khan, M. A. H.; Shallcross, D. E. Direct Gas-Phase Formation of Formic Acid through Reaction of Criegee Intermediates with Formaldehyde. *Commun. Chem.* **2023**, *6* (1), 1–10. https://doi.org/10.1038/s42004-023-00933-2.
(26) Liu, Y.; Bayes, K. D.; Sander, S. P. Measuring Rate Constants for Reactions of the Simplest Criegee Intermediate (CH_2OO) by Monitoring the OH Radical. *J. Phys. Chem. A* **2014**, *118* (4), 741–747. https://doi.org/10.1021/jp407058b.
(27) Kuo, M.; Takahashi, K.; Lin, J. J. Reactions of Criegee Intermediates Are Enhanced by Hydrogen-Atom Relay Through Molecular Design. *ChemPhysChem* **2020**, *21* (18), 2056–2059. https://doi.org/10.1002/cphc.202000585.
(28) Tadayon, S. V.; Foreman, E. S.; Murray, C. Kinetics of the Reactions between the Criegee Intermediate CH_2OO and Alcohols. *J. Phys. Chem. A* **2018**, *122* (1), 258–268. https://doi.org/10.1021/acs.jpca.7b09773.
(29) McGillen, M. R.; Curchod, B. F. E.; Chhantyal-Pun, R.; Beames, J. M.; Watson, N.; Khan, M. A. H.; McMahon, L.; Shallcross, D. E.; Orr-Ewing, A. J. Criegee Intermediate–Alcohol Reactions, A Potential Source of Functionalized Hydroperoxides in the Atmosphere. *ACS Earth Space Chem.* **2017**. https://doi.org/10.1021/acsearthspacechem.7b00108.
(30) Kawamura, K.; Okuzawa, K.; Aggarwal, S. G.; Irie, H.; Kanaya, Y.; Wang, Z. Determination of Gaseous and Particulate Carbonyls (Glycolaldehyde, Hydroxyacetone, Glyoxal, Methylglyoxal, Nonanal and Decanal) in the Atmosphere at Mt. Tai. *Atmos. Chem. Phys.* **2013**, *13* (10), 5369–5380. https://doi.org/10.5194/acp-13-5369-2013.

(31) Clair, J. M. St.; Spencer, K. M.; Beaver, M. R.; Crounse, J. D.; Paulot, F.; Wennberg, P. O. Quantification of Hydroxyacetone and Glycolaldehyde Using Chemical Ionization Mass Spectrometry. *Atmos. Chem. Phys.* **2014**, *14* (8), 4251–4262. https://doi.org/10.5194/acp-14-4251-2014.
(32) Grosjean, D.; Williams, E. L.; Grosjean, E. Atmospheric Chemistry of Isoprene and of Its Carbonyl Products. *Environ. Sci. Technol.* **1993**, *27* (5), 830–840. https://doi.org/10.1021/es00042a004.
(33) Mellouki, A.; Wallington, T. J.; Chen, J. Atmospheric Chemistry of Oxygenated Volatile Organic Compounds: Impacts on Air Quality and Climate. *Chem. Rev.* **2015**, *115* (10), 3984–4014. https://doi.org/10.1021/cr500549n.
(34) Xing, Y.; Li, H.; Huang, L.; Wu, H.; Shen, H.; Chen, Z. The Production of Formaldehyde and Hydroxyacetone in Methacrolein Photooxidation: New Insights into Mechanism and Effects of Water Vapor. *Journal of Environmental Sciences* **2018**, *66*, 1–11. https://doi.org/10.1016/j.jes.2017.05.037.
(35) Taatjes, C. A.; Liu, F.; Rotavera, B.; Kumar, M.; Caravan, R.; Osborn, D. L.; Thompson, W. H.; Lester, M. I. Hydroxyacetone Production From C_3 Criegee Intermediates. *J. Phys. Chem. A* **2017**, *121* (1), 16–23. https://doi.org/10.1021/acs.jpca.6b07712.
(36) Johnson, T. J.; Profeta, L. T. M.; Sams, R. L.; Griffith, D. W. T.; Yokelson, R. L. An Infrared Spectral Database for Detection of Gases Emitted by Biomass Burning. *Vib. Spectrosc.* **2010**, *53* (1), 97–102. https://doi.org/10.1016/j.vibspec.2010.02.010.
(37) Weise, D. R.; Johnson, T. J.; Reardon, J. Particulate and Trace Gas Emissions from Prescribed Burns in Southeastern U.S. Fuel Types: Summary of a 5-Year Project. *Fire Safety J.* **2015**, *74*, 71–81. https://doi.org/10.1016/j.firesaf.2015.02.016.
(38) Dagaut, P.; Liu, R.; Wallington, T. J.; Kurylo, M. J. Kinetic Measurements of the Gas-Phase Reactions of Hydroxyl Radicals with Hydroxy Ethers, Hydroxy Ketones, and Keto Ethers. *J. Phys. Chem.* **1989**, *93* (23), 7838–7840. https://doi.org/10.1021/j100360a022.
(39) Orlando, J. J.; Tyndall, G. S.; Fracheboud, J.-M.; Estupiñan, E. G.; Haberkorn, S.; Zimmer, A. The Rate and Mechanism of the Gas-Phase Oxidation of Hydroxyacetone. *Atmos. Environ.* **1999**, *33* (10), 1621–1629. https://doi.org/10.1016/S1352-2310(98)00386-0.
(40) Aschmann, S. M.; Arey, J.; Atkinson, R. Atmospheric Chemistry of Selected Hydroxycarbonyls. *J. Phys. Chem. A* **2000**, *104* (17), 3998–4003. https://doi.org/10.1021/jp9939874.
(41) Chowdhury, P. K.; Upadhyaya, H. P.; Naik, P. D.; Mittal, J. P. ArF Laser Photodissociation Dynamics of Hydroxyacetone: LIF Observation of OH and Its Reaction Rate with the Parent. *Chem. Phys. Lett.* **2002**, *351* (3), 201–207. https://doi.org/10.1016/S0009-2614(01)01377-X.
(42) Butkovskaya, N. I.; Pouvesle, N.; Kukui, A.; Mu, Y.; Le Bras, G. Mechanism of the OH-Initiated Oxidation of Hydroxyacetone over the Temperature Range 236–298 K. *J. Phys. Chem. A* **2006**, *110* (21), 6833–6843. https://doi.org/10.1021/jp056345r.
(43) Dillon, T. J.; Horowitz, A.; Hölscher, D.; Crowley, J. N.; Vereecken, L.; Peeters, J. Reaction of HO with Hydroxyacetone ($HOCH_2C(O)CH_3$): Rate Coefficients (233–363 K) and Mechanism. *Phys. Chem. Chem. Phys.* **2006**, *8* (2), 236–246. https://doi.org/10.1039/B513056E.
(44) Baasandorj, M.; Griffith, S.; Dusanter, S.; Stevens, P. S. Experimental and Theoretical Studies of the Kinetics of the OH + Hydroxyacetone Reaction As a Function of Temperature. *J. Phys. Chem. A* **2009**, *113* (39), 10495–10502. https://doi.org/10.1021/jp904238w.
(45) Bedjanian, Y. Temperature-Dependent Kinetic Study of the Reaction of Hydroxyl Radicals with Hydroxyacetone. *J. Phys. Chem. A* **2020**, *124* (14), 2863–2870. https://doi.org/10.1021/acs.jpca.0c00429.
(46) Vu, N. D.; Khamaganov, V.; Nguyen, V. S.; Carl, S. A.; Peeters, J. Absolute Rate Coefficient of the Gas-Phase Reaction between Hydroxyl Radical (OH) and Hydroxyacetone: Investigating the Effects of Temperature and Pressure. *J. Phys. Chem. A* **2013**, *117* (47), 12208–12215. https://doi.org/10.1021/jp407701z.

(47) *IUPAC – Task Group on Atmospheric Chemical Kinetic Data Evaluation*. https://iupac.aeris-data.fr/ (accessed 2023-06-23).
(48) Baker, J.; Arey, J.; Atkinson, R. Rate Constants for the Gas-Phase Reactions of OH Radicals with a Series of Hydroxyaldehydes at 296 ± 2 K. *J. Phys. Chem. A* **2004**, *108* (34), 7032–7037. https://doi.org/10.1021/jp048979o.
(49) El Dib, G.; Sleiman, C.; Canosa, A.; Travers, D.; Courbe, J.; Sawaya, T.; Mokbel, I.; Chakir, A. First Experimental Determination of the Absolute Gas-Phase Rate Coefficient for the Reaction of OH with 4-Hydroxy-2-Butanone (4H2B) at 294 K by Vapor Pressure Measurements of 4H2B. *J. Phys. Chem. A* **2013**, *117* (1), 117–125. https://doi.org/10.1021/jp3074909.
(50) Messaadia, L.; El Dib, G.; Lendar, M.; Cazaunau, M.; Roth, E.; Ferhati, A.; Mellouki, A.; Chakir, A. Gas-Phase Rate Coefficients for the Reaction of 3-Hydroxy-2-Butanone and 4-Hydroxy-2-Butanone with OH and Cl. *Atmos. Environ.* **2013**, *77*, 951–958. https://doi.org/10.1016/j.atmosenv.2013.06.028.
(51) Bouzidi, H.; Aslan, L.; El Dib, G.; Coddeville, P.; Fittschen, C.; Tomas, A. Investigation of the Gas-Phase Photolysis and Temperature-Dependent OH Reaction Kinetics of 4-Hydroxy-2-Butanone. *Environ. Sci. Technol.* **2015**, *49* (20), 12178–12186. https://doi.org/10.1021/acs.est.5b02721.
(52) Cheramangalath Balan, R.; Rajakumar, B. Photo-Oxidation Reaction Kinetics and Mechanistics of 4-Hydroxy-2-Butanone with Cl Atoms and OH Radicals in the Gas Phase. *J. Phys. Chem. A* **2019**, *123* (20), 4342–4353. https://doi.org/10.1021/acs.jpca.9b00995.
(53) Keller-Rudek, H.; Moortgat, G. K.; Sander, R.; Sörensen, R. The MPI-Mainz UV/VIS Spectral Atlas of Gaseous Molecules of Atmospheric Interest. *Earth Syst. Sci. Data* **2013**, *5*, 365–373. https://doi.org/10.5194/essd-5-365-2013.
(54) Petitjean, M.; Reyès-Pérez, E.; Pérez, D.; Mirabel, Ph.; Le Calvé, S. Vapor Pressure Measurements of Hydroxyacetaldehyde and Hydroxyacetone in the Temperature Range (273 to 356) K. *J. Chem. Eng. Data* **2010**, *55* (2), 852–855. https://doi.org/10.1021/je9004905.
(55) Lindenmaier, R.; Tipton, N.; Sams, R. L.; Brauer, C. S.; Blake, T. A.; Williams, S. D.; Johnson, T. J. Assignment of the Fundamental Modes of Hydroxyacetone Using Gas-Phase Infrared, Far-Infrared, Raman, and *Ab Initio* Methods: Band Strengths for Atmospheric Measurements. *J. Phys. Chem. A* **2016**, *120* (30), 5993–6003. https://doi.org/10.1021/acs.jpca.6b05045.
(56) Schmidt, M. W.; Baldridge, K. K.; Boatz, J. A.; Elbert, S. T.; Gordon, M. S.; Jensen, J. H.; Koseki, S.; Matsunaga, N.; Nguyen, K. A.; Su, S.; et al. General Atomic and Molecular Electronic Structure System. *J. Comput. Chem.* **1993**, *14* (11), 1347–1363. https://doi.org/10.1002/jcc.540141112.
(57) Gordon, M. S.; Schmidt, M. W. Advances in Electronic Structure Theory: GAMESS a Decade Later. In *Theory and Applications of Computational Chemistry, the First Forty Years*; Dykstra, C. E., Frenking, G., Kim, K. S., Scuseria, G. E., Eds.; Elsevier: Amsterdam, 2005; Vol. Chapter 41, pp 1167–1189.
(58) Gaussian 16, Revision B.01, Frisch, M. J.; Trucks, G. W.; Schlegel, H. B.; Scuseria, G. E.; Robb, M. A.; Cheeseman, J. R.; Scalmani, G.; Barone, V.; Petersson, G. A.; Nakatsuji, H.; et al.. Gaussian, Inc., Wallingford CT, 2016.
(59) Barca, G. M. J.; Bertoni, C.; Carrington, L.; Datta, D.; De Silva, N.; Deustua, J. E.; Fedorov, D. G.; Gour, J. R.; Gunina, A. O.; Guidez, E.; et al.. Recent Developments in the General Atomic and Molecular Electronic Structure System. *J. Chem. Phys.* **2020**, *152* (15), 154102. https://doi.org/10.1063/5.0005188.
(60) Montgomery, J. A.; Frisch, M. J.; Ochterski, J. W.; Petersson, G. A. A Complete Basis Set Model Chemistry. VI. Use of Density Functional Geometries and Frequencies. *J. Chem. Phys.* **1999**, *110* (6), 2822–2827. https://doi.org/10.1063/1.477924.
(61) Xu, X.; Alecu, I. M.; Truhlar, D. G. How Well Can Modern Density Functionals Predict Internuclear Distances at Transition States? *J. Chem. Theory Comput.* **2011**, *7* (6), 1667–1676. https://doi.org/10.1021/ct2001057.

(62) Schenker, S.; Schneider, C.; Tsogoeva, S. B.; Clark, T. Assessment of Popular DFT and Semiempirical Molecular Orbital Techniques for Calculating Relative Transition State Energies and Kinetic Product Distributions in Enantioselective Organocatalytic Reactions. *J. Chem. Theory Comput.* **2011**, *7* (11), 3586–3595. https://doi.org/10.1021/ct2002013.
(63) Simmie, J. M.; Somers, K. P. Benchmarking Compound Methods (CBS-QB3, CBS-APNO, G3, G4, W1BD) against the Active Thermochemical Tables: A Litmus Test for Cost-Effective Molecular Formation Enthalpies. *J. Phys. Chem. A* **2015**, *119* (28), 7235–7246. https://doi.org/10.1021/jp511403a.
(64) Zhan, C.-G.; Nichols, J. A.; Dixon, D. A. Ionization Potential, Electron Affinity, Electronegativity, Hardness, and Electron Excitation Energy: Molecular Properties from Density Functional Theory Orbital Energies. *J. Phys. Chem. A* **2003**, *107* (20), 4184–4195. https://doi.org/10.1021/jp0225774.
(65) Messaadia, L.; El Dib, G.; Ferhati, A.; Roth, E.; Chakir, A. Gas Phase UV Absorption Cross-Sections for a Series of Hydroxycarbonyls. *Chem. Phys. Lett.* **2012**, *529*, 16–22. https://doi.org/10.1016/j.cplett.2012.01.044.
(66) J. B. Burkholder, S. P. Sander, J. Abbatt, J. R. Barker, C. Cappa, J. D. Crounse, T. S. Dibble, R. E. Huie, C. E. Kolb, M. J. Kurylo, et al. *"Chemical Kinetics and Photochemical Data for Use in Atmospheric Studies, Evaluation No. 19,"* JPL Publication 19-5, Jet Propulsion Laboratory, Pasadena, 2019 Http://Jpldataeval.Jpl.Nasa.Gov; 19; 2019.
(67) Foreman, E. S.; Kapnas, K. M.; Jou, Y.; Kalinowski, J.; Feng, D.; Gerber, R. B.; Murray, C. High Resolution Absolute Absorption Cross Sections of the $\tilde{B}^1A'$–$\tilde{X}^1A'$ Transition of the CH_2OO Biradical. *Phys. Chem. Chem. Phys.* **2015**, *17* (48), 32539–32546. https://doi.org/10.1039/C5CP04977F.
(68) Spietz, P.; Gómez Martín, J. C.; Burrows, J. P. Spectroscopic Studies of the I_2/O_3 Photochemistry: Part 2. Improved Spectra of Iodine Oxides and Analysis of the IO Absorption Spectrum. *J. Photochem. Photobio. A* **2005**, *176* (1–3), 50–67. https://doi.org/10.1016/j.jphotochem.2005.08.023.
(69) Laidler, K. J. *Chemical Kinetics*, 3rd ed.; Harper & Row: New York, 1987.
(70) Debnath, A.; Rajakumar, B. Investigation of Kinetics and Mechanistic Insights of the Reaction of Criegee Intermediate (CH_2OO) with Methyl-Ethyl Ketone (MEK) under Tropospherically Relevant Conditions. *Chemosphere* **2023**, *312*, 137217. https://doi.org/10.1016/j.chemosphere.2022.137217.
(71) Watson, N. A. I.; Black, J. A.; Stonelake, T. M.; Knowles, P. J.; Beames, J. M. An Extended Computational Study of Criegee Intermediate–Alcohol Reactions. *J. Phys. Chem. A* **2019**, *123* (1), 218–229. https://doi.org/10.1021/acs.jpca.8b09349.
(72) Aroeira, G. J. R.; Abbott, A. S.; Elliott, S. N.; Turney, J. M.; Schaefer, H. F. The Addition of Methanol to Criegee Intermediates. *Phys. Chem. Chem. Phys.* **2019**, *21* (32), 17760–17771. https://doi.org/10.1039/C9CP03480C.
(73) Kuo, M.-T.; Yang, J.-N.; Lin, J. J.-M.; Takahashi, K. Substituent Effect in the Reactions between Criegee Intermediates and 3-Aminopropanol. *J. Phys. Chem. A* **2021**, *125* (30), 6580–6590. https://doi.org/10.1021/acs.jpca.1c03737.
(74) Buras, Z. J.; Elsamra, R. M. I.; Jalan, A.; Middaugh, J. E.; Green, W. H. Direct Kinetic Measurements of Reactions between the Simplest Criegee Intermediate CH_2OO and Alkenes. *J. Phys. Chem. A* **2014**, *118* (11), 1997–2006. https://doi.org/10.1021/jp4118985.
(75) Eskola, A. J.; Döntgen, M.; Rotavera, B.; Caravan, R. L.; Welz, O.; Savee, J. D.; Osborn, D. L.; Shallcross, D. E.; Percival, C. J.; Taatjes, C. A. Direct Kinetics Study of CH_2OO + Methyl Vinyl Ketone and CH_2OO + Methacrolein Reactions and an Upper Limit Determination for CH_2OO + CO Reaction. *Phys. Chem. Chem. Phys.* **2018**, *20* (29), 19373–19381. https://doi.org/10.1039/C8CP03606C.

(76) Zhou, X.; Chen, Y.; Liu, Y.; Li, X.; Dong, W.; Yang, X. Kinetics of CH_2OO and Syn-CH_3CHOO Reaction with Acrolein. *Phys. Chem. Chem. Phys.* **2021**, *23* (23), 13276–13283. https://doi.org/10.1039/D1CP00492A.
(77) Novelli, A.; Hens, K.; Tatum Ernest, C.; Martinez, M.; Nölscher, A. C.; Sinha, V.; Paasonen, P.; Petäjä, T.; Sipilä, M.; Elste, T.; et al. Estimating the Atmospheric Concentration of Criegee Intermediates and Their Possible Interference in a FAGE-LIF Instrument. *Atmos. Chem. Phys.* **2017**, *17* (12), 7807–7826. https://doi.org/10.5194/acp-17-7807-2017.
(78) Finlayson-Pitts, B. J.; Pitts, J. N. *Chemistry of the Upper and Lower Atmosphere: Theory, Experiments, and Applications*; Academic Press: San Diego, 2000.
(79) Seinfeld, J. H.; Pandis, S. N. *Atmospheric Chemistry and Physics: From Air Pollution to Climate Change*; Wiley, 2012.

TOC graphic